Energetics of Double-Ion Occupancy in the Gramicidin A Channel

Yuhui Li,[†] Olaf S. Andersen,[‡] and Benoît Roux*,[†]

Department of Biochemistry and Molecular Biology, University of Chicago, Chicago, Illinois 60637, United States, and Department of Physiology and Biophysics, Weill Cornell Medical College, New York, New York 10021, United States

Received: June 23, 2010; Revised Manuscript Received: September 8, 2010

To understand the energetics of double-ion occupancy in gramicidin A (gA) channels, the 2D potential of mean force (PMF) is calculated for two ions at different positions along the channel axis. The cross sections of this 2D PMF are compared with available one-ion PMFs to highlight the effect of one ion on the permeation dynamics of the other. It is found that, if the first ion stays on one side in the channel, the second ion has to pass over an additional barrier to move into the outer binding site. At the same time, both outer and inner binding sites for the second ion become shallower than those in the one-ion PMF. The calculated ion−ion repulsion for a doubly occupied channel is about 2 kcal/mol, in good agreement with previous experimental estimates. The number of water molecules inside the channel and their dipole moment are calculated to interpret the energetics of double-ion occupancy. As the first ion moves into the outer binding site and then further into the channel, the oxygen atoms of the single-file water column in the channel are oriented to point toward the ion. The observed dipole moment distribution of a singly occupied channel has only one sharp peak, and the water alignment is essentially perfect once the ion is in the inner binding site. For this reason, there is an energy penalty to accommodate a second ion at the opposite end of the channel.

Introduction

The possibility that biological membrane channels could be occupied by more than one permeant ion simultaneously was first recognized in 1955 by Hodgkin and Keynes,[1] who showed, using unidirectional ion-flux measurements, that the effective permeant unit in the K^+ channel in axons of the cuttlefish *Sepia officinalis* was a multimer of 2−3 ions. Decades later, the X-ray structure of the KcsA potassium channel revealed the configuration of the narrow selectivity filter with multiple specific K^+ binding sites.[2,3] Building on the structure of the KcsA channel, a wide array of simulation methods were then used to computationally dissect the various energetic factors at play in the narrow selectivity filter.[4−11] More recently, computational methods have reached the relevant time scale allowing for the direct brute-force simulation of permeation events.[12]

Computational studies on KcsA support the concept that ion−ion repulsion is an essential component of the mechanism by which K^+ channels succeed in achieving high selectivity while maintaining a large ionic conductance. This was particularly exemplified by the calculation of the multi-ion potential of mean force (PMF), showing that the exit of the outermost K^+ ion is strongly correlated with the translocation of the other K^+ in the selectivity filter,[9] though the dense packing of K^+ and water in the selectivity filter complicates the quantitative interpretation of those results. However, while MD simulations of K^+ channels of ever-increasing complexity are possible, issues of permeation and selectivity are partly obscured by the inherent complexities associated with inactivation and conformational flexibility of the pore.[13,14] For this reason, it becomes instructive to quantitatively characterize the importance of ion−ion interactions in the context of a simpler transmembrane pore.

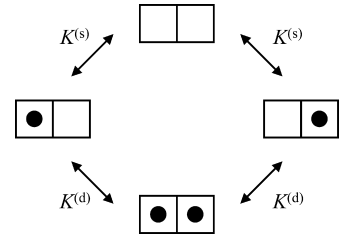

Figure 1. Simple generic two-ion scheme, comprising four states of channel occupancy with their respective equilibrium constants.

The channels formed by the pentadecapeptide gramicidin A (gA), which have over the years become "the" prototypical model system of choice for computational studies of ion permeation, are particularly attractive. The structure of this small channel has been determined to atomic resolution using nuclear magnetic resonance (NMR) in detergent micelles in solution[15−17] and in oriented lipid bilayer membranes.[18] It is well understood that ions and water molecules cannot pass each other along the narrow pore and that permeation must proceed through a single-file translocation mechanism.[19]

The gA channel is only moderately selective among monovalent cations, but is impermeable to divalent cations and anions.[19,20] It has two cation binding sites, which are located near the entrance at each ends of the dimer channel, about 20 Å apart.[21−23] At low permeant cation concentrations, only one of the two binding sites is occupied, whereas the two sites may be occupied simultaneously at high concentration.[19,24] At high cation concentrations, when the channel is doubly occupied, the preferred ion binding positions are further apart than at low concentrations, when the channel is singly occupied.[23] The two-ion state diagram for ion occupancy within the channel thus can be described as in Figure 1.[25,26] By virtue of its structural and chemical simplicity, the gA channel has been the object of numerous computational studies[20,27−30] (see refs 31 and 32 for

* To whom correspondence should be addressed. E-mail: roux@uchicago.edu.
[†] University of Chicago.
[‡] Weill Cornell Medical College.

10.1021/jp105820u
Published on Web 10/12/2010

reviews). It can serve as a very useful model system to study the principles governing ion−ion repulsion in the confined environment of a narrow molecular pore.

Several lines of evidence indicate that it can be occupied simultaneously by two monovalent cations.[19,24,33] One might be led to believe that, because the binding sites are separated by about 20 Å, ion−ion interactions in the doubly occupied gA can be understood in simple terms. However, the situation is more complicated than this.[34] Interpretation of ion flux data indicates that double occupancy is relatively more favorable for the large K^+, Rb^+, and Cs^+ cations than for the small Li^+ and Na^+ cations.[19,34] While this trend cannot be explained on the basis of simple considerations, a computational study based on free energy perturbation molecular dynamics (FEP/MD) simulations of singly and doubly occupied channels indicated that the doubly occupied state was indeed relatively more favorable for the larger ions, in qualitative agreement with experimental observations.[34] Analysis of the FEP/MD simulations revealed that a crucial factor was strong ion−water correlations within the hydrogen-bonded water chain located inside the narrow pore. It is important to realize that such FEP/MD simulations, in which the type of ions is alchemically transformed, only report on the relative thermodynamic stability of the system with the bound ions. These calculations do not provide information about the microscopic processes associated with the occurrence of single and double occupancy. A more powerful theoretical approach consists in computing the multi-ion PMF.[35] So far, only one MD study reported the calculation of a PMF pertaining to double occupancy;[30] however, only a subset of the full two-ion PMF, restricted to configurations in which the two ions move symmetrically along the pore axis on both side of the channel, was calculated. The complete free energy landscape governing the occurrence of double occupancy has never been characterized using computational methods.

The goal of the present study, therefore, is to explore the microscopic factors governing double-ion occupancy in the gA channel. To do so, we use potential of mean force (PMF) umbrella sampling techniques to characterize the complete free energy surface governing the relative movement of two K^+ ions in the neighborhood of the gA channel.

Methods

Single-stranded gA dimers were constructed using the 1JNO coordinates.[17] This structure was employed because it has been shown to agree with a range of experimental solution and solid-state NMR experiments.[36] The channel was embedded in a bilayer membrane consisting of one shell of phospholipids, comprising 20 dimyristoylphosphatidylcholine (DMPC) molecules. Hexagonal periodic boundaries with a translation length of 32.1 Å in the *xy*-plane were imposed. The dimensions of the periodic box was fixed in the *xy* dimensions. Pressure coupling was employed in the *z*-direction, which was parallel to the normal of the membrane with average height ∼75 Å. The concentration of the ionic solution, KCl, was set to 1 M. This relatively high concentration was chosen to achieve better sampling. On the basis of experimental data,[23,33] one would expect some fraction of doubly occupied channel at this salt concentration. However, it should be noted that this cannot occur in the present calculations because the state of occupancy of the channel in the MD simulations is controlled by excluding all the ions that are not explicitly involved in the PMF umbrella sampling simulations from a spherical region of radius 14 Å (relative to the center of mass of the dimer).[20,28,29]

The program CHARMM was used for all MD simulations with the PARAM27 force field and TIP3P water model.[37] The tryptophan residues were represented by the refined force field from Macias and MacKerell, in which the partial atomic charges, Lennard-Jones parameters, and force constants were modified according to ab initio calculations.[38] Particle-mesh Ewald,[39] SHAKE,[40] and constant pressure and temperature algorithms[41] were employed in all simulations.

To compare the potential of mean force (PMF) for single ion occupancy to that for double-ion occupancy, we proceeded as follows: first, the MD simulations for single ion occupancy were carried out with umbrella sampling.[42] The ion was held by the window potential $w_i(z) = {}^1/_2K_i(z - z_i)^2$ (with $K_i = 10$ kcal/mol/Å ^{2}) at 0.5 Å increments in $z = (-20,20)$ Å. Configurations taken from previous PMF calculations of K^+ in the gA channel using PARAM27[20,28,29] were used to initiate the umbrella sampling MD simulations. For each window, after energy minimization and 80 ps equilibration simulation with the new tryptophan force field, the next 2 ns trajectories were used for the PMF calculation.

The initial configurations for the double-ion-occupancy simulations were generated by exchanging a water molecule located closest to the desired position with the aqueous cation furthest from the channel in the available one-ion-occupancy configurations. Because the size of a K^+ ion is nearly the same as that of water molecule, the effect of steric hindrance on the ion−water exchanging can be neglected. Using umbrella sampling, we simulated 625 independent windows positioned at 0.5 Å increments in $z_1 = (-20,-8)$ Å and $z_2 = (8,20)$ Å for the left and right cation, respectively. (We limited the exploration to this part of the total configuration space because ions and water are in a strict single-file organization in the central pore, -8 Å $\le z \le 8$ Å.) The umbrella potential for the two ions is taken as $w_{i,j} = {}^1/_2K_{i,j}[(z_1 - z_i)^2 + (z_2 - z_j)^2]$, where z_i and z_j are the window positions and $K_{i,j} = 10$ kcal/mol/Å^2. For each window, energy minimization and equilibration were performed for 80 ps before calculating the 2 ns trajectories used for the calculation of PMF. The ion distributions were unbiased using the weighted histogram analysis method (WHAM).[43] The two-ion 2D PMF is symmetrized by creating duplicate windows on opposite sides of the channel.

Both one-ion and two-ion PMFs are calculated using umbrella sampling in the constant pressure and temperature ensemble. The one-ion PMF, $\mathscr{W}(\mathbf{r}_1)$, can be evaluated as a configurational integral

$$e^{-\mathscr{W}(\mathbf{r}_1)/k_BT} = \frac{\int' d\mathbf{r}_2 \ldots \int' d\mathbf{r}_N \int d\mathbf{X}\, e^{-U(\mathbf{r}_1,\mathbf{r}_2,\ldots\mathbf{r}_N;\mathbf{X})/k_BT}}{\int' d\mathbf{r}_2 \ldots \int' d\mathbf{r}_N \int d\mathbf{X}\, e^{-U(\mathbf{r'}_1,\mathbf{r}_2,\ldots\mathbf{r}_N;\mathbf{X})/k_BT}} \quad (1)$$

where k_B is Boltzmann's constant, T is the temperature, and U is the potential energy as a function of ionic coordinates $\mathbf{r}_1$, $\mathbf{r}_2$, ..., $\mathbf{r}_N$ and all other degrees of freedom $\mathbf{X}$ (protein, lipid, and water). The primes on the integral denotes that the ions 2 to N are restricted to be located in the bulk (they cannot enter the channel region). An offset reference $\mathscr{W}(\mathbf{r'}_1) = 0$ is set when $\mathbf{r}_1'$ is far away in the bulk in bulk.

The coordinate along the channel axis (z) of the ion is chosen as the reaction coordinate to describe the permeation processes. After some algebraic derivation, the one-ion 1D PMF $\mathscr{W}'(z)$ can be evaluated as an integral

$$e^{-\mathscr{W}(z)/k_BT} = \frac{1}{(\pi R^2)} \int dx\, dy\, H_{cyl}(x,y) e^{-[\mathscr{W}(x,y,z)-\mathscr{W}(0,0,z')]/k_BT} \quad (2)$$

where R is the radius of a flat-bottom cylindrical constraint to restrict the ion lateral displacement (we use $R = 8$ Å and force constant 10 kcal/mol/Å^2 in the simulation similar to previous study[20,28,29]), H_{cyl} is a Heaviside step function, which represents the cylindrical constraint. Its value is 1 inside the restraining cylinder, and 0 outside. The 1D PMF is offset so that $\mathscr{W}'(z)$ goes to zero when z is far away in the bulk region.

Through a similar derivation, the two-ion PMF can be written as

$$e^{-\mathscr{W}(z_1,z_2)/k_BT} = \frac{1}{(\pi^2 R^4)} \int dx_1\, dy_1\, dx_2\, dy_2\, H_{cyl}(x_1,y_1,x_2,y_2) \times e^{-[\mathscr{W}(x_1,y_1,z_1,x_2,y_2,z_2)-\mathscr{W}(0,0,z'_1,0,0,z'_2)]/k_BT} \quad (3)$$

where the subscripts 1 and 2 represent the two cations that are considered explicitly. In the derivation, the bulk reference has a definite value that is independent of the sampling time.

The calculation of equilibrium binding constants and the presence of a cylindrical restraint deserve a few comments. The methodology used here relies on the calculation of a PMF along some coordinate that controls the translocation of the ligand from the binding pocket to the bulk solution. Such a PMF-based approach was originally designed to treat the binding of a phosphotyrosine peptide, a flexible molecular ligand, to a SH2 domain.[44] The present calculations represent a special and relatively simple case: the binding of a monatomic ligand (a K^+ ion) to a protein. It may be noted that the PMF-based approach for computing the equilibrium binding constant differs from the somewhat more familiar alchemical FEP methods involving the decoupling of the ligand from its surrounding (binding pocket or bulk solution).[45−48] The decoupling FEP approach is typically the method of choice in the case of a neutral ligand that binds to a deeply buried site,[46,49−51] whereas the PMF-based approach is most useful in the case of a charged ligand that associates with a solvent-exposed site.[44,52] Both the PMF-based and the FEP decoupling approaches can rely on multiple restraining potentials introduced to improve and guarantee convergence. This causes no problems as long as the effects of the restraints are rigorously accounted for to produce unbiased estimates (for a review, see ref 53). Here, a flat-bottom cylindrical restraining potential is introduced to impose an upper bound on the lateral displacements of the K^+ ion in the bulk phase during the umbrella sampling simulations. This is needed to construct mathematically well-defined PMFs along the channel axis.[28,54] Other choices of restraining potential could be used, although the final results will be independent of such choice only if the computations are properly unbiased.[54]

Results and Discussion

Two-Ion Potential of Mean Force. Figure 2a shows the symmetrized two-ion 2D PMF $\mathscr{W}(z_1,z_2)$, which is calculated using 2 ns simulation/window. The reference value $\mathscr{W} = 0$ is set as both the cations are located far away in the bulk: $z_1 = -20$ Å and $z_2 = 20$ Å. In the one-ion PMF,[28] there are two binding sites in each half of the channel: a deeper outer binding site at $z = \pm 11.3$ Å and a shallower inner binding site at $z = \pm 9.4$ Å. The 2D PMF (Figure 2) is divided into six regions by dashes based on its topography and symmetry about the diagonal. Snapshots of typical configurations found in the six regions are shown in Figure 2b under the PMF. For simplicity, only the channel, the permeating cations, and the water molecules in the channel and at the entrances are shown. Region i corresponds to a flat region where the PMF varies between −0.05 and 1.2 kcal/mol. In this region (snapshot i), both cations are outside the channel and the water molecules form a single-file column inside the channel. Regions ii and iii are troughs, with region ii being deeper than region iii. The PMF in region ii varies between −2.2 and 0 kcal/mol, and the PMF in region iii varies between −1.2 and 0 kcal/mol. The free energy minimum of the map, −2.2 kcal/mol, is at (−11.3 Å, 20 Å) in region ii. Snapshots ii and iii show the configurations in which one cation is in the bulk and the other is in the outer binding and the inner binding site, respectively. Region iv is a basin with a depth of −1.8 kcal/mol. The configurations in this basin have both cations located in the outer binding sites, as shown in snapshot iv. The basin in region iv is shallower than the trough in region ii, indicating that the outer site's binding energy cannot compensate the interaction between the two cations when both cations are in outer binding sites. Region v is also a basin with a depth of −1.2 kcal/mol which is shallower than the basin in region iv. The left cation is located in the outer binding site and the right cation in the inner binding site, as shown in snapshot v. In region vi there are two hills with heights of 2.6 and 6.1 kcal/mol, respectively. The lower hill is at (−10.3 Å, 10.3 Å) corresponding to a configuration with both ions located on the barrier between the outer and inner binding sites. There is the higher hill at (−8 Å, 8 Å) where the two cations are closest to each other in the investigated region. Snapshot vi displays the configuration of both the cations in

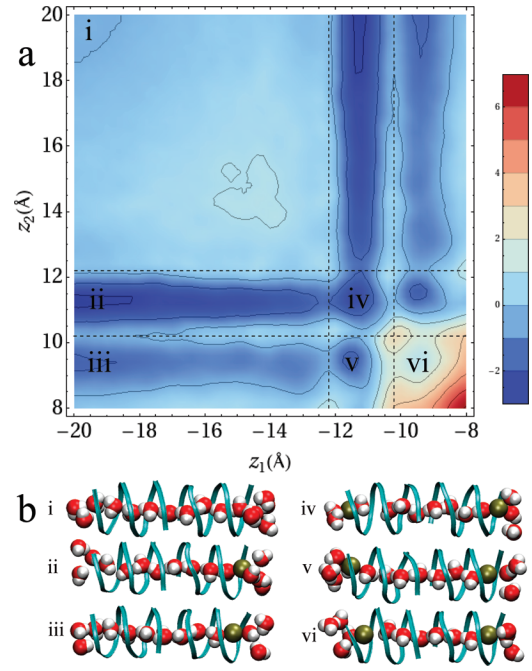

Figure 2. (a) 2D PMF for a doubly occupied gA channel is divided into six regions based on the shape of the 2D energy plot (two of the regions, ii and iii, are disconnected; only one of the subregions is labeled). $z = 0$ is the center of the channel. The 2D PMF is symmetric with respect to the diagonal from top-right to bottom-left. (b) Snapshots of the typical configurations in the six regions: i, both cation are in bulk; ii/iii, the left cation is located at the outer/inner binding site and the right one is in bulk; iv, both the cations are in the outer binding sites; v, the left cation is located at the inner binding site and the right one at the outer binding site; vi, both the cations are in the inner binding sites.

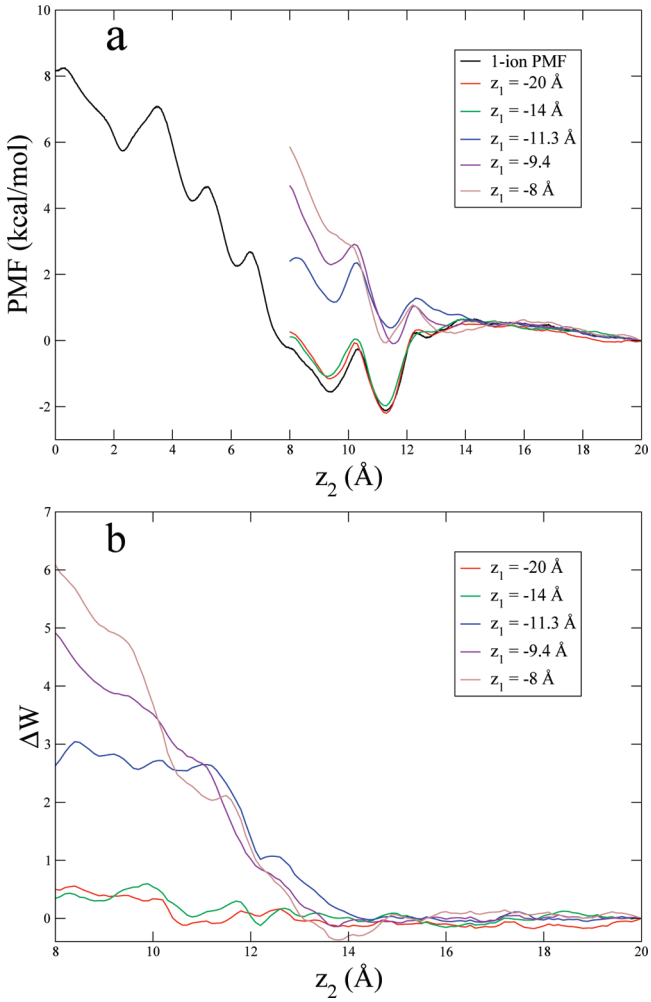

Figure 3. Comparison of the cross sections of the two-ion 2D PMF with the one-ion PMF. The cross sections are chosen at $z_1 = -20$, -14, -11.3, -9.4, -8 Å. (a) The cross sections of the two-ion 2D PMF and the one-ion PMF. (b) The net effect of the presence of the second ion at fixed positions, determined by subtracting the one-ion PMF from each of the cross sections of the 2D PMF.

the inner binding sites. Due to the short distance between the two cations, there is nearly no free energy basin in the vicinity of (−9.4 Å, 9.4 Å) in region vi.

To illustrate the details of the ion−ion interactions, selected cross sections of the two-ion 2D PMF are shown in Figure 3a. For each cross section, the reference $\mathscr{W} = 0$ is for the right cation in bulk ($z_2 = 20$ Å), such that the PMF comparison has the physical meaning of one ion entering the channel on the right while the other one is at a fixed position on the left. When the left ion is in the bulk at $z_1 = -20$ Å, the two-ion PMF nearly coincides with one-ion PMF, which is expected because the left cation is far away from the channel. Surprisingly, however, even when the left cation is near the left entrance ($z_1 = -14$ Å) but further away from the channel center than the outer binding site, the cross section of the 2D PMF roughly overlaps with the one-ion PMF, which means the left cation has a very weak effect on the right ion's movement into the inner binding site. When the left cation stays in the outer binding site at $z_1 = -11.3$ Å, a free energy peak begins to appear just outside the outer binding site at $z_2 = 12.2$ Å. The peak persists when the left ion moves into the inner binding site at $z_1 = -9.4$ and further into the channel at -8 Å. These peaks correspond to the peaks in the 2D PMF in Figure 2 along $z_2 = 12.2$ Å. The potential basins of the outer binding site (for the right ion) become much shallower as the left ion is deeper in the channel, at $z_1 = -11.3$, -9.4, and -8 Å. The new peak at $z_2 = 12.2$ Å and the shallower outer binding site indicate that, if one ion enters the channel and stays inside, the second ion must cross an energy barrier to enter a less stable outer binding site. Also, the inner binding site (for the right cation) becomes shallower when the left cation moves further inside the channel, from $z_1 = -11.3$ to -9.4 Å, and it vanishes when the left cation is at $z_1 = -8$ Å. The PMFs increase steeply, compared to the one-ion PMF when the right ion moves further into the channel if the left ion is at $z_1 = -9.4$ and -8 Å. The main reasons are that the number of the water molecules between the two cations is fixed once both cations reside deeply inside the channel, and this water molecule single file is incompressible.

To show more clearly the net effect of the left cation being at different fixed positions, the one-ion PMF is subtracted from the cross sections of the two-ion 2D PMF. The curves in Figure 3b are calculated as $\Delta\mathscr{W}(z_1,z_2) = \mathscr{W}(z_1,z_2) - \mathscr{W}(z_1,z_2 = \infty)$. All the curves fluctuate around 0 in the region 14 Å $\leq z_2 \leq$ 20 Å, indicating that the left cation has little effect on the PMF of the right cation as long as it stays outside the channel ($z_2 \geq 14$ Å). When the left cation is outside the channel, -20 Å $\leq z_1 \leq -14$ Å, it has a very weak effect with only a 0.5 kcal/mol increase in the PMF of the right cation at $z_2 = 8$ Å. When the left cation is in the outer binding site, at $z_1 = -11.3$ Å the PMF of the right cation increases steeply as the right cation moves into the channel (11.3 Å $\leq z_2 \leq$ 14 Å). Then the difference PMF reaches a plateau (2.7 kcal/mol) as the right cation moves further into the channel ($z_2 \leq 11.3$ Å). When the left cation is located in the inner binding site, at $z_1 = -9.4$ Å, or at $z_1 = -8$ Å, the difference PMFs are similar to that observed when the left cation is in the outer binding site, at $z_1 = -11.3$ Å, in the region (11.3 Å $\leq z_2 \leq$ 14 Å). As the right cation moves deeper into the channel (8 Å $\leq z_2 \leq$ 11.3 Å), the changes in the PMFs become more pronounced, with the largest changes observed when the left cation is at -8 Å.

Assuming that the changes in the PMFs are due solely to electrostatic interactions between the ions, it is possible to extract an "effective" dielectric constant $\varepsilon(z_1, z_2)$ between the two cations using to the equation

$$\Delta\mathscr{W}(z_1, z_2) \approx \frac{1}{4\pi\varepsilon_0\varepsilon(z_1, z_2)}\frac{q_1 q_2}{|z_1 - z_2|} \tag{4}$$

As a reference, the dielectric constant in the bulk region is ∼80 for the TIP3P water model. Equation 4 is obviously a very rough approximation because there should also be contributions from the water packing between the two ions. For this reason, values of effective dielectric constant were extracted by simple visual inspection of the ion−ion PMF repulsion $\Delta\mathscr{W}(z_1,z_2)$. Based on $\Delta\mathscr{W}$ in Figure 3b, the "effective" dielectric constant $\varepsilon(z_1, z_2)$ is estimated when the right cation is located in the channel ($z_2 \leq$ 12.2 Å). When the left cation is between -20 and -14 Å, $\varepsilon(z_1, z_2)$ is ∼25 when the right cation stays in the inner binding site (8 Å $\leq z_2 \leq$ 10.2 Å). In the case of the left cation being within the channel ($z_1 = -11.3$, -9.4, and -8 Å), the $\varepsilon(z_1, z_2)$ curves are nearly flat in the range 8 Å $\leq z_2 \leq$ 12.2 Å, with $\varepsilon(z_1, z_2)$ for $z_1 = -11.3$, -9.4, and -8 Å being ∼5.5, 4.2 and 3.6, respectively. When both cations are in the channel, the "effective" dielectric constant is much smaller than the dielectric constant in the bulk region. Its value decreases as the distance between the two cations decreases, probably because the water between the ions become increasingly organized. It should be

emphasized that the above values do not represent actual microscopic dielectric constants, and are only meant as a guide for the magnitude of the ion−ion electrostatic shielding that is at play in the channel.

It is of interest to characterize the relative magnitude of the equilibrium binding constants, $K^{(s)}$ and $K^{(d)}$, corresponding to the single and double states of occupancy as defined in the simple two-ion scheme depicted in Figure 1. Although the PMF calculations were carried out in the presence of a flat-bottom cylindrical restraint,[20,28,29] it is possible to account for the artificial bias introduced by the cylindrical restraining potential to obtain rigorous and unbiased estimates about the 1- and two-ion equilibrium binding processes.[54] For instance, the single-ion equilibrium binding constant $K^{(s)}$ can be expressed in terms of the one-ion PMF as,[28]

$$K^{(s)} = (\pi R^2) \int_{z_{min}}^{z_{max}} dz\, e^{-\mathscr{W}(z)/k_B T} \quad (5)$$

where R is the radius of the bounding cylinder used to calculate the one-ion PMF and the binding site is defined to be within the range $z_{min} \le z \le z_{max}$ along the axial direction. (The expression requires that $\mathscr{W}(z)$ be zero when z is far away in the bulk). The equilibrium binding constant leading to the doubly occupied channel, $K^{(d)}$, can be written as

$$\begin{aligned} K^{(d)} &= \frac{(\pi^2 R^4) \int_{z_{1,min}}^{z_{1,max}} dz_1 \int_{z_{2,min}}^{z_{2,max}} dz_2\, e^{-\mathscr{W}(z_1,z_2)/k_B T}}{(\pi R^2) \int_{z_{min}}^{z_{max}} dz\, e^{-\mathscr{W}(z)/k_B T}} \\ &= \frac{1}{K^{(s)}} (\pi^2 R^4) \int_{z_{1,min}}^{z_{1,max}} dz_1 \int_{z_{2,min}}^{z_{2,max}} dz_2\, e^{-\mathscr{W}(z_1,z_2)/k_B T} \end{aligned} \quad (6)$$

where the binding sites for the first ion and second ion are defined to be within the range -12.4 Å $\le z_1 \le -8$ Å and 8 Å $\le z_2 \le 12.4$ Å, respectively, along the axial direction. (The expression requires that $\mathscr{W}(z_1,z_2)$ be offset to zero when both z_1 and z_2 are far away in the bulk.) Using the cross section of the two-ion PMF at $z_1 = 20$ Å, the single-ion dissociation constant is calculated as 0.30 M. Given this value, the dissociation constant for the second ion is 8.24 M using the two-ion 2D PMF. The equilibrium binding constant can be used to determine an effective ion−ion repulsion. Accordingly, the free energy cost of binding one ion in the doubly occupied state relative to the singly occupied state is

$$\Delta G = -k_B T \ln\left[\frac{K^{(d)}}{K^{(s)}}\right] \quad (7)$$

This equation yields a value of 1.98 kcal/mol for the effective ion−ion repulsion between 2 K^+ bound to the gA channel.

This result from computations can be compared with previous experimental estimates. Jing and Urry measured the association of ions to gA channels bound to DPC micelles using solution NMR.[23] The measurements could clearly distinguish a tight and weak binding constant, corresponding to the association of a first and then a second ion. For K^+, the binding constants $K^{(s)}$ and $K^{(d)}$ are 60 and 3 M^{-1}, respectively. This leads to an estimated ion−ion repulsion of 1.8 kcal/mol. Remarkably, the magnitude of the repulsion does not appear to be highly sensitive to the type of cation. It is estimated to be 1.4 kcal/mol for Na^+, 2.1 kcal/mol for Rb^+, and 1.80 kcal/mol for Cs^+.[23] These results can be compared with those of Becker et al.,[33] who extracted a complete set of rate constants from measurements of K^+ ion conduction through the gA channel incorporated into a lipid membrane. The complete kinetic analysis was based on the so-called 3B2S2I-(IP,DL) scheme. The latter corresponds to an Eyring hopping rate model with 3 barriers (3B), 2 sites (2S), and 2 ions (2I), which is also augmented to account for interfacial polarization (IP) as well as access diffusion limitation (DL).[33] The effective equilibrium binding constants $K^{(s)}$ and $K^{(d)}$ determined from the ratio of the association and dissociation rate constant are 3.67 and 0.25 M^{-1}, respectively, yielding an estimated ion−ion repulsion of 1.6 kcal/mol for K^+.

The present result of 1.98 kcal/mol, calculated from the one-ion and two-ion PMFs, is in excellent agreement with those experimental estimates. Notably, there is considerable improvement relative to the value of 6 kcal/mol for two Na^+ from an earlier MD study.[34] A number of factors may be responsible for the improvement, including the usage of an all-atom force field, the presence of an explicit phospholipid bilayer membrane with bulk solvent, and the increased sampling efficiency afforded by the two-ion PMF method. The previous result was obtained using an alchemical charging free energy perturbation (FEP) method, and the MD simulations were based on a reduced system with an extended atom force field representation.[34] The good agreement with the present results indicates that the long-range ion−ion electrostatic interactions incorporated in the all-atom model are sound.

Number of Water Molecules and the Dipole Moment Fluctuation. The water molecules inside the channel play an important role in ion permeation.[28] To understand the mechanism of permeation, the number and the dipole moment of the water molecules between the two cations, and inside the channel, were investigated.

Based on the two-ion PMF and the positions of the outer and inner binding sites, the z coordinate of the cation is grouped into three regions: bulk region (12.2 Å $\le z \le$ 20 Å), the outer binding site region (10.2 Å $\le z <$ 12.2 Å), and the inner binding site region (8 Å $\le z_2 <$ 10.2 Å). In Figure 4 the number of water molecules, n, is plotted as the left cation stays in each of the specific regions and the right one moves from the bulk region to the inner binding site region. When the left cation is in bulk water (Figure 4a), there are 8 water molecules inside the channel when the right cation is in bulk. If the right cation is in the outer binding site, n fluctuates between 7 and 8. When the ion moves into the inner binding site region, n has a maximum at $n = 7$ with a shoulder at $n = 6$. This indicates that 1 or 2 water molecules originally inside the channel are expelled as the right cation moves into the channel. In some trajectories with both cations located at the channel entrances (-14 Å $\le z_1 \le -12$ Å and 12 Å $\le z_2 \le$ 14 Å), water molecules are observed to pass around the cation and move into or out of the channel. In the case of the left cation being in the outer binding site region (Figure 4b), the number of water molecules fluctuates between 7 and 8 when the right cation is in the bulk region or the outer binding site region. When the right cation is in the inner binding site region, n decreases to 6 or 7 because the distance between the ions becomes shorter. When the left cation is in the inner binding site region (Figure 4c), the number of water molecules decreases from 7 to 6 as the right ion moves from outside to inside the channel. If both cations are inside the inner binding site, the peak n is at 6 with a shoulder at 5.

The distributions of the dipole moment of the water column between the two cations (and inside the channel) were also

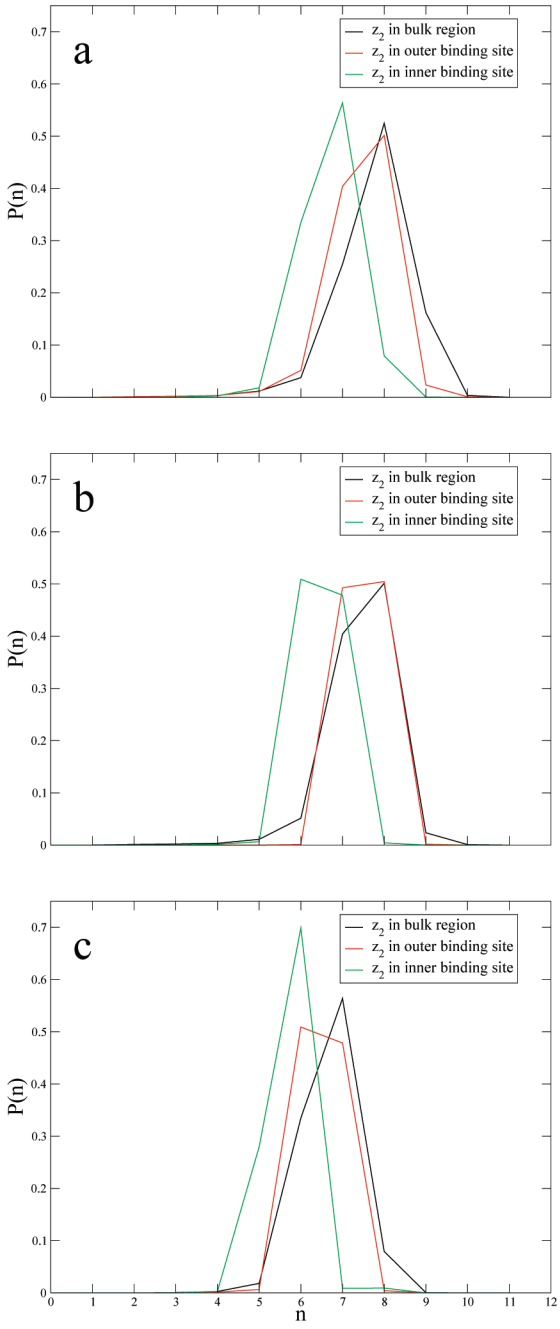

Figure 4. Number of water molecules inside the channel. The left cation is in (a) the bulk region, (b) the outer binding site, and (c) the inner binding site.

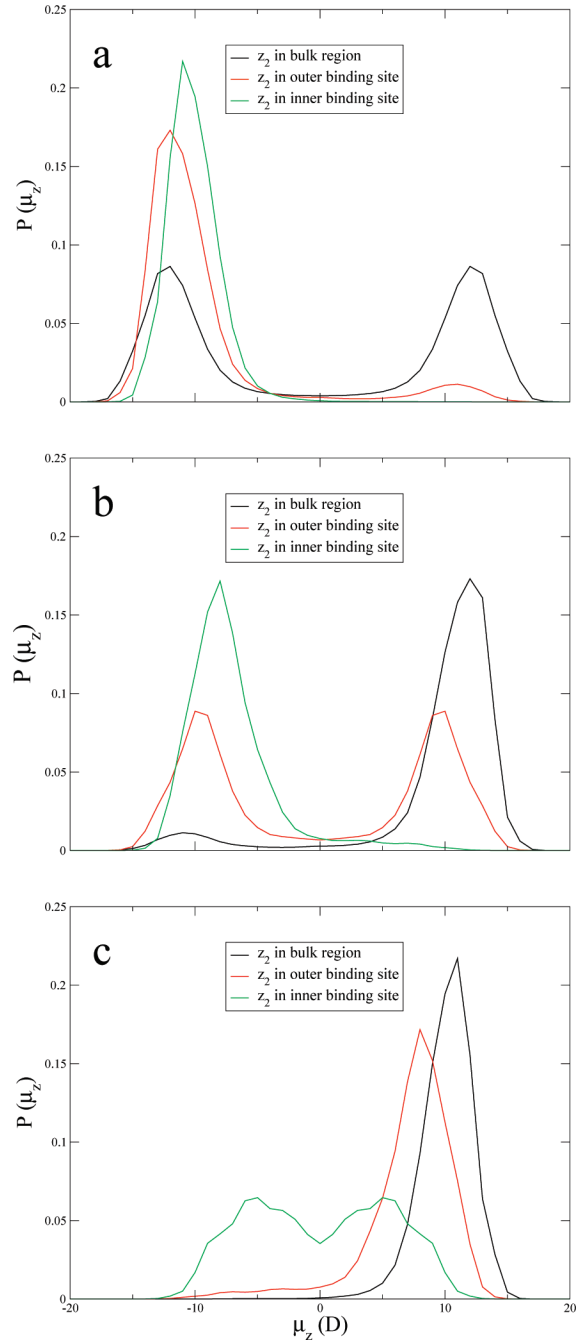

Figure 5. Dipole of water molecules inside the channel. The left cation is in (a) the bulk region, (b) the outer binding site, and (c) the inner binding site.

calculated. In Figure 5a, the distribution is shown for the left cation being in bulk. When both cations are in the bulk region, the water molecules inside the channel are connected by hydrogen bonds to form a single-file column, as shown in snapshot i in Figure 2. There are two possible dipole moment orientations for the single-file water column, ±12 D. The dipole moment distribution is symmetrical with respect to $\mu_z = 0$ (the black curve in Figure 5a). The dipole moment distributions are symmetrical if the two cations are located symmetrically with respect to $z = 0$ (the red curve in Figure 5b, the green curve in Figure 5c). Under these situations, the left and right cations have the same strong interactions with the single-file water molecules inside the channel, but the interactions have opposite directions, which results in the dipole moment being smaller but with the same probability of being at μ_z and $-\mu_z$.

If the left cation is located in the bulk region and the right cation is in the outer binding site region, the preferred configuration has the water at the end of the single-file column with its oxygen pointing toward the right cation as shown in snapshot ii in Figure 2. Therefore, the dipole distribution peak (the red curve in Figure 5a) at −12 D becomes much higher than the peak at 12 D. The dipole moment of the water molecules has a greater probability of being at $\mu_z < 0$ than at $\mu_z > 0$. As the right cation moves further into the inner binding site, the single-file water has a more aligned structure (shown in snapshot iii in Figure 2) so that the peak (in green) around $\mu_z = -11$ D is the highest and the peak around $\mu_z = 11$ D disappears. When the left cation occupies the outer binding site and the right cation stays in bulk region, a higher peak of the distribution is located at 12 D while a much lower peak is

located at −12 D, which means that the oxygen of the water at the end of the single-file column faces the left cation most of the time. A symmetrical distribution (the red curve in Figure 5b) is obtained while both cations are in the outer binding site region (shown in snapshot iv in Figure 2) and the peaks of this distribution are at ±10 D. When the right cation is in the inner binding site region, which is closer to the channel center than the left outer binding site region, the oxygen of the water at the right end of the single-file column turns to face the right cation as shown in snapshot v in Figure 2. Therefore, the distribution function has only one peak at −8 D. If the left cation is in the inner binding site region, the peaks of the distributions are located at 11 and 8 D when the right cation is in the bulk and in the outer binding site, respectively. When both cations are in inner binding sites, the distribution function is symmetric with peaks at ±5 D and an increased possibility at $\mu_z = 0$. In this case, there is only a small number of water molecules, 5 or 6, between the two cations. Both cations interact strongly with these water molecules, so that the water single-file column flips more frequently. The dipole moment has greater probability in a state of $\mu_z = 0$ than in the previous situations.

Figure 5 shows that, if one cation stays inside the channel (the outer binding site region or even deeper, in the inner binding site region) and the other one is outside the channel, the distribution functions have just one sharp peak. This is because the cation deep inside the channel has stronger interactions with the single-file water column than the cation in the outer binding site region or outside the channel. When the second cation moves into the channel and stays at the symmetric position to the first one, the distribution will have two peaks, which are symmetric about $\mu_z = 0$. When the second cation moves deeper into the channel than the first cation, the single-file water column will favor the stabilization of the second cation. Thus the distribution function will have a sharp peak. This indicates that the single-file water column needs to flip, fully or partly, to enable the second cation moving into the channel. Figure 5 also shows that, when the left cation is confined to a region, the probability distribution peaks at $\mu > 0$ become lower and the peaks at $\mu < 0$ become higher, as the right cation moves from bulk region into the outer binding site region and then further into the inner binding site region.

Conclusion

Using umbrella sampling, we calculated the two-ion 2D PMF through the gA channel, which shows the free energy basins for double occupancy. In the comparison between the cross sections of double-ion 2D PMF and the single-ion PMF, the influence of double-ion occupancy on the PMF becomes apparent. When the first ion stays outside the channel, it has a very weak effect on the second ion because of long distance between the two ions. When the first ion is located in the channel, a new energy barrier appears for the second ion, as it moves into the channel and the outer and inner binding sites become much shallower. The PMFs also become steeper as the second ion moves deeper into the channel. These results indicate that the ions inside the channel have a strong effect on the other ion. When both ions are in the channel, the "effective" dielectric constant is much smaller than the dielectric constant in the bulk region. Its value decreases as the distance between the two ions decreases, which shows that the effect of double-ion occupancy is important when both ions are located inside the channel. The free energy of binding an ion in the doubly occupied state relative to the singly occupied state is computed, and its value agrees very well with the experimental value.

The number of water molecules inside the channel and their dipole moment were calculated to interpret the energetics of double-ion occupancy in gA channels. When one ion moves into the channel, one water molecule is expelled from the channel. The dipole moment of the single-file water column plays an important role in understanding the double-ion occupancy. When the first ion occupies the (outer or inner) binding site or is further into the channel, the preferred state has the water at the end of the single-file water column with its oxygen atoms pointing toward it. The observed dipole moment distribution has only one sharp peak, which means that there is a higher energy barrier to flip the single-file water column completely or to partially stabilize the second ion than in the case of the first ion being outside the channel. When the second ion moves into the channel and stays at the symmetric position of the first ion, the single-file column of water flips frequently. When the second ion moves further into the channel than the first ion, the single-file water column will flip to favor the stabilization of the second ion.

Acknowledgment. This work was supported by Grant GM070971 from the National Institutes of Health.

References and Notes

(1) Hodgkin, A. L.; Keynes, R. D. *J. Physiol. (London)* **1955**, *128*, 61–88.
(2) Doyle, D. A.; Cabral, J. M.; Pfuetzner, R. A. A.; Kuo, J. M. G.; Cohen, S. L.; Chait, B. T.; MacKinnon, R. *Science* **1998**, *280*, 69–77.
(3) Zhou, Y.; Morais-Cabral, J. H.; Kaufman, A.; MacKinnon, R. *Nature* **2001**, *414*, 43–48.
(4) Guidoni, L.; Torre, V.; Carloni, P. *Biochemistry* **1999**, *38*, 8599–8604.
(5) Bernèche, S.; Roux, B. *Biophys. J.* **2000**, *78*, 2900–2917.
(6) Allen, T. W.; Bliznyuk, A.; Rendell, A. P.; Kuyucak, S.; Chung, S. H. *J. Chem. Phys.* **2000**, *112*, 8191–8204.
(7) Åqvist, J.; Luzhkov, V. B. *Nature* **2000**, *404*, 881–884.
(8) Shrivastava, I. H.; Sansom, M. S. *Biophys. J.* **2000**, *78*, 557–570.
(9) Bernèche, S.; Roux, B. *Nature* **2001**, *414*, 73–77.
(10) Noskov, S. Y.; Berneche, S.; Roux, B. *Nature* **2004**, *431*, 830–834.
(11) Khalili-Araghi, F.; Tajkhorshid, E.; Schulten, K. *Biophys. J.* **2006**, *91*, L72–74.
(12) Jensen, M. Ø.; Borhani, D. W.; Lindorff-Larsen, K.; Maragakis, P.; Jogini, V.; Eastwood, M. P.; Dror, R. O.; Shaw, D. E. *Proc. Natl. Acad. Sci.* **2010**, *107*, 5833–5838.
(13) Berneche, S.; Roux, B. *Structure* **2005**, *13*, 591–600.
(14) Cordero-Morales, J. F.; Jogini, V.; Lewis, A.; Vásquez, V.; Cortes, D. M.; Roux, B.; Perozo, E. *Nat. Struct. Mol. Biol.* **2007**, *14*, 1062–1069.
(15) Arseniev, A. S.; Barsukov, I. L.; Bystrov, V. F.; Lomize, A. L.; Ovchinnikov, Y. A. *FEBS Lett.* **1985**, *186*, 168–174.
(16) Arseniev, A. S.; Barsukov, I. L.; Bystrov, V. F.; Ovchinnikov, Y. A. *Biol. Membr.* **1986**, *3*, 437–462.
(17) Townsley, L. E.; Tucker, W. A.; Sham, S.; Hinton, J. F. *Biochemistry* **2001**, *40*, 11676–11686.
(18) Ketchem, R. R.; Roux, B.; Cross, T. A. *Structure* **1997**, *5*, 1655–1669.
(19) Andersen, O. S.; Koeppe, R. E., II *Physiol. Rev.* **1992**, *72*, S89–S158.
(20) Allen, T. W.; Andersen, O. S.; Roux, B. *Biophys. Chem.* **2006**, *124*, 251–267.
(21) Urry, D. W.; Walker, J. T.; Trapane, T. L. *J. Membr. Biol.* **1982**, *69*, 225–231.
(22) Olah, G. A.; Huang, H. W.; Liu, W.; Wu, Y. *J. Mol. Biol.* **1991**, *218*, 847–858.
(23) Jing, N.; Prasad, K. U.; Urry, D. W. *Biochim. Biophys. Acta* **1995**, *1238*, 1–11.
(24) Schagina, L. V.; Grinfeldt, A. E.; Lev, A. A. *Nature* **1978**, *273*, 243–245.
(25) Urban, B. W.; Hladky, S. B.; Haydon, D. A. *Biochim. Biophys. Acta* **1980**, *602*, 331–354.
(26) Andersen, O. S. *Methods Enzymol.* **1989**, *171*, 62–112.
(27) Allen, T. W.; Bastug, T.; Kuyucak, S.; Chung, S. H. *Biophys. J.* **2003**, *84*, 2159–2168.
(28) Allen, T. W.; Andersen, O. S.; Roux, B. *Proc. Natl. Acad. Sci.* **2004**, *101*, 117–122.

(29) Allen, T. W.; Andersen, O. S.; Roux, B. *Biophys. J.* **2006**, *90*, 3447–3468.
(30) Bastug, T.; Kuyucak, S. *J. Chem. Phys.* **2007**, *126*, 105103–105112.
(31) Roux, B.; Karplus, M. *Annu. Rev. Biomol. Struct. Dyn.* **1994**, *23*, 731–761.
(32) Roux, B. *Acc. Chem. Res.* **2002**, *35*, 366–375.
(33) Becker, M. D.; Koeppe, R. E., II; Andersen, O. S. *(Biophys. Discuss.) Biophys. J.* **1992**, *62*, 25–27.
(34) Roux, B.; Prod'hom, B.; Karplus, M. *Biophys. J.* **1995**, *68*, 876–892.
(35) Roux, B.; Allen, T. W.; Berneche, S.; Im, W. *Q. Rev. Biophys.* **2004**, *37*, 15–103.
(36) Allen, T. W.; Andersen, O. S.; Roux, B. *J. Am. Chem. Soc.* **2003**, *125*, 9868–9877.
(37) Jorgensen, W. L.; Chandrasekhar, J.; Madura, J. D.; Inpey, R. W.; Klein, M. L. *J. Chem. Phys.* **1983**, *79*, 926–935.
(38) Macias, A. T.; MacKerell, A. D., Jr. *J. Comput. Chem.* **2005**, *26*, 1452–1463.
(39) Darden, T.; York, D.; Pedersen, L. *J. Chem. Phys.* **1993**, *98*, 10089–10092.
(40) Ryckaert, J. P.; Ciccotti, G.; Berendsen, H. J. C. *J. Comput. Chem.* **1977**, *23*, 327–341.
(41) Feller, S. E.; Zhang, Y.; Pastor, R. W.; Brooks, B. R. *J. Chem. Phys.* **1995**, *103*, 4613–4621.
(42) Torrie, G. M.; Valleau, J. P. *J. Comput. Physiol.* **1977**, *23*, 187–199.
(43) Kumar, S.; Bouzida, D.; Swendsen, R. H.; Kollmam, P. A.; Rosenberg, J. M. *J. Comput. Chem.* **1992**, *13*, 1011–1021.
(44) Woo, H.; Roux, B. *Proc. Natl. Acad. Sci. U.S.A.* **2005**, *102*, 6825–6830.
(45) Roux, B.; Nina, M.; Pomes, R.; Smith, J. *Biophys. J.* **1996**, *71*, 670–681.
(46) Hermans, J.; Wang, L. *J. Am. Chem. Soc.* **1997**, *119*, 2707–2714.
(47) Gilson, M.; Given, J.; Bush, B.; McCammon, J. A. *Biophys. J.* **1997**, *72*, 1047–1069.
(48) Boresch, S.; Tettinger, F.; Leitgeb, M.; Karplus, M. *J. Phys. Chem. B* **2003**, *107*, 9535–9551.
(49) Deng, Y.; Roux, B. *J. Chem. Theor. Comput.* **2006**, *2*, 1255–1273.
(50) Wang, J.; Deng, Y.; Roux, B. *Biophys. J.* **2006**, *91*, 1798–2814.
(51) Mobley, D. L.; Chodera, J. D.; Dill, K. A. *J. Chem. Phys.* **2006**, *125*, 084902.
(52) Gan, W.; Roux, B. *Proteins* **2009**, *74*, 996–1007.
(53) Deng, Y. Q.; Roux, B. *J. Phys. Chem. B* **2009**, 2234–2246.
(54) Roux, B.; Andersen, O. S.; Allen, T. W. *J. Chem. Phys.* **2008**, *128*, 227101; author reply page 227102.

JP105820U